Statistics and Computing (2021) 31:60
https://doi.org/10.1007/s11222-021-10035-5

Fast generation of Gaussian random fields for direct numerical simulations of stochastic transport

D. I. Palade[1] · **M. Vlad**[1]

Received: 14 April 2020 / Accepted: 26 July 2021 / Published online: 15 August 2021

Abstract
We propose a novel discrete method of constructing Gaussian Random Fields based on a combination of modified spectral representations, Fourier and Blob. The method is intended for Direct Numerical Simulations of the V-Langevin equations. The latter are stereotypical descriptions of anomalous stochastic transport in various physical systems. From an Eulerian perspective, our method is designed to exhibit improved convergence rates. From a Lagrangian perspective, our method offers a pertinent description of particle trajectories in turbulent velocity fields: the exact Lagrangian invariant laws are well reproduced. From a computational perspective, the computing time is reduced by a factor of two in comparison with Fourier-like or Blob-like methods and an order of magnitude in comparison with FFT algorithms.

Keywords Gaussian random field · Stochastic · Direct simulation · V-Langevin

1 Introduction

Stochastic phenomena are ubiquitous in nature and laboratory, being present in various sciences: physics and chemistry Kampen 2007, biology Bressloff 2014, finances Paul 2013, social sciences Diekmann and Mitter 2014, etc. In particular, physical stochastic processes such as turbulent flows Monin 1971, anomalous transport in fusion plasmas Balescu 2007, 2005, flows through porous media Ganapathysubramanian and Zabaras 2009, seismic motion Liu et al. 2019 are complex phenomena that are modeled by nonlinear stochastic (partial) differential equations Boivin et al. 1998. Most of the theoretical studies Manfredi and Dendy 1996; Reuss and Misguich 1996; Radivojević and Akhmatskaya 2020; Naulin et al. 1999 are based on direct numerical simulations (DNSs) (or Monte Carlo simulations). Unfortunately, the ensemble statistics for the input processes as well as for the solutions exhibit slow convergence rates, with fluctuations that decay, usually, as $M^{-1/2}$, where M is the dimension of the ensemble (the number of realizations). Thus, the numerical effort involved in a DNS is a matter of concern, even in the context of the computing power available nowadays Yang and Shen 2017.

The present paper belongs to this broad interdisciplinary research area. More precisely, we discuss methods for constructing Gaussian random fields (GRFs) that could be of interest in a wide spectrum of domains and provide insights into the stochastic transport described by V-Langevin equations. The latter are the most general type of first-order Langevin equations: $\dot{\mathbf{x}}(t) = \mathbf{v}[\mathbf{x}(t), t]$, with $\mathbf{x}(t)$ the trajectory and $\mathbf{v}(\mathbf{x}, t)$ a random "velocity" field. It describes the general problem of diffusion by continuous movements (the extension of the Brownian motion to the space-correlated stochastic velocity fields). This approach is widely used for describing the turbulent transport or the stochastic advection process in fluids Pozorski and Minier 1998; Haworth and Pope 1986; Kraichnan 1976; Monin 1971, laboratory plasmas Naulin et al. 1999; Balescu et al. 1994; Tautz and Dosch 2013; Manfredi and Dendy 1996 or astrophysical plasmas Zimbardo et al. 1995; Vlad et al. 2015.

The V-Langevin eqns., as well as many other stochastic models, require input stochastic processes $\mathbf{v}(\mathbf{x}, t)$ represented by Gaussian random fields (GRFs) Abrahamsen 1997. Thus, when performing a DNS we need to generate a large ensemble of fields, which makes an important fraction of the computing time. The topic of GRFs representations is old and has been studied in a variety of fields of research such as plasma turbulence Balescu 2007; Manfredi and Dendy

✉ D. I. Palade
dragos.palade@inflpr.ro

[1] National Institute of Laser, Plasma and Radiation Physics, PO Box MG 36, 077125 Măgurele, Bucharest, Romania

1996; Tautz 2012; Boivin et al. 1998, spatial statistics Krishnamachari and Chellappa 1997; Won et al. 1996; Wong 1969; Chan and Wood 1999; Bevilacqua and Gaetan 2015; Higdon 2002; Hoef et al. 2004, pattern recognition and machine learning Ghahramani and Hinton 2000; Hofmann et al. 2008.

Consequently, a large amount of constructing techniques are available Liu et al. 2019; Cuevas et al. 2020; Solin and Särkkä 2020; Tautz and Dosch 2013. In the context of DNSs of V-Langevin eqns. Balescu (2007); Manfredi and Dendy (1996); Tautz (2012); Boivin et al. (1998), the most employed are the spectral methods of discrete Fourier decomposition Liu et al. 2019 implemented using the fast Fourier transform (FFT) algorithms. A complementary spectral representation, familiar to other fields such as geo-statistics, is the Moving-Average method Hoef et al. 2004; Ravalec et al. 2000. Unfortunately, using FFT-like algorithms, i.e., equidistant grids, leads to a series of drawbacks: mathematically, the resulting fields and their covariance functions are periodic, a feature that is not usually required by the statistical model; computationally, the convergence of the statistical properties is slow; physically, invariants of motion may be altered due to in-between grid points interpolation. The solution is to use randomly distributed grids.

The aim of the present study is to derive analytically and test numerically a few classes of approximations related to the Fourier and Moving-Average (which we shall call "Blob") methods. In particular, we explore their abilities for V-Langevin problems. Finally, we propose a novel, hybrid, Fourier-Blob method able to improve the computational time of DNSs of transport problems by an order of magnitude factor in comparison with standard FFT algorithms and a factor of two in comparison with more refined Fourier-like or Blob-like approaches.

The theoretical results are presented in Sect. 2. Starting from general, integral, representations of a GRF, we derive discrete approximations. They are modified by introducing additional random elements, which are expected to improve the convergence. Two particular types of representations are chosen (Fourier- and Blob-like), which are shown to be canonically conjugated.

Section 3 contains a detailed study of the accuracy of these discrete representations. Three variants of the Fourier and Blob representation are considered. Their ability to reproduce the characteristics of the GRFs is numerically analyzed at two levels. The basic level consists of a comparison of the results on the standard Eulerian quantities (covariance and distribution functions). The second level involves the DNS of a special test-particle advection process: particle stochastic motion in two-dimensional, incompressible, time-independent velocity fields. This is a Hamiltonian process with two Lagrangian invariants. One appears in each trajectory (local invariant), and the other involves the distribution of the Lagrangian velocity (statistical invariant). They provide strong benchmarks for the numerical simulation and, implicitly, for the GRF generation method. The results on the diffusion coefficients and on the distribution of the displacements are also compared. Finally, this detailed analysis permitted to find the hybrid Fourier-Blob method, which appears as being roughly twice as fast as pure Fourier or Blob generators in DNS studies of complex stochastic advection processes. The conclusions are summarized in Sect. 4.

2 Theory

We consider a real GRF $\phi(\mathbf{x})$ on a d dimensional space $\phi : \mathbb{R}^d \to \mathbb{R}$ with zero average $\langle\phi(\mathbf{x})\rangle = 0$ and covariance function $\mathcal{E}(\mathbf{x};\mathbf{y}) = \langle\phi(\mathbf{x})\phi(\mathbf{y})\rangle$, where $\langle\cdot\rangle$ is the statistical averaging operation. This field can be generally represented through a set of parametric functions $\{F(\mathbf{x};\mathbf{s})\}$ as:

$$\phi(\mathbf{x}) = \int d\mathbf{s} F(\mathbf{x};\mathbf{s})\zeta(\mathbf{s}) \tag{1}$$

$$\mathcal{E}(\mathbf{x};\mathbf{y}) = \int d\mathbf{s} F(\mathbf{x};\mathbf{s})F(\mathbf{y};\mathbf{s}) \tag{2}$$

where $\zeta(\mathbf{s})$ is an uncorrelated random variable $\langle\zeta(\mathbf{s})\zeta(\mathbf{s}')\rangle = \delta(\mathbf{s}-\mathbf{s}')$. It can be easily proven that Eqs. (1), (2) reproduce the correct covariance function $\mathcal{E}(\mathbf{x};\mathbf{y})$, while its Gaussian character is guaranteed by the Central Limit Theorem. Before discussing the nature of the parametric functions $F(\mathbf{x};\mathbf{s})$, let us address the matter of discreteness.

It is tempting to pass from the integral representation (1), (2) to a finite and discrete form in two steps: truncate and discretize the domain of integration. As we shall see, the operator $F(\mathbf{x};\mathbf{s})$ can be, usually, safely neglected outside some finite domain in the $\mathbf{s}$ space so the truncation is justified. But using a Riemann sum $\int d\mathbf{s} \to \sum_{\mathbf{s}}$ to approximate the integrals in Eqs. (1), (2) might not be the best approach (in the sense of errors, smoothness and convergence).

2.1 Discrete representations

Let us define in the $\mathbb{R}^d$ parametric space $\{\mathbf{s}\}$ an equidistant grid of points $\{\mathbf{s}_0\}$ with the interspacing L, such that each point $\mathbf{s}_0$ is centered in the hypercubic domain $\mathcal{D}(\mathbf{s}_0)$ of volume L^d. Accordingly, the integral over parameters can be broken as:

$$\int d\mathbf{s} \equiv \sum_{\mathbf{s}_0} \int_{\mathcal{D}(\mathbf{s}_0)} d\mathbf{s}.$$

Considering that $F(\mathbf{x};\mathbf{s})$ are infinitely differentiable, one can Taylor expand around a grid point $\mathbf{s}_0$

$$F(\mathbf{x};\mathbf{s}) = \sum_n \frac{(\mathbf{s}-\mathbf{s_0})^n}{n!}\nabla^n_{\mathbf{s_0}} F(\mathbf{x};\mathbf{s}_0),$$

and the field (1) can be written

$$\phi(\mathbf{x}) = \sum_{\mathbf{s}_0}\left(\sum_n \frac{\hat{\alpha}_n}{n!}\nabla^n_{\mathbf{s}_0}\right) F(\mathbf{x};\mathbf{s}_0),$$

where the coefficients

$$\hat{\alpha}_n = \int_{\mathcal{D}(\mathbf{0})} d\mathbf{s}\zeta(\mathbf{s})\mathbf{s}^n$$

are random with zero average and correlation $\langle\hat{\alpha}_n\hat{\alpha}_m\rangle \propto L^{2d}(L/2)^{n+m+1}/(n+m+1)$. In essence, we pass from an integral (dense) representation (1) to a discrete one by recasting the dense character in an infinite series of random variables $\hat{\alpha}_n$. In the limit $L \to 0$, we can cut the series at the first-order $\mathcal{O}(L^2)$ and approximate:

$$\phi(\mathbf{x}) \approx \sum_{\mathbf{s}_0} \alpha_0 F(\mathbf{x};\mathbf{s}_0 + \mathbf{fi}) \tag{3}$$

where α_0 is a Gaussian variable with L^d variance, while $\mathbf{fi}$ a Cauchy distributed variable with the scale parameter $L/\sqrt{12}$. The representation (3) reproduces the correlation only in an approximate manner (dependent on the magnitude of L). Also, the density of points

$$\rho = \sum_{\mathbf{s}_0}\langle\delta[\mathbf{x}-(\mathbf{s}_0+\mathbf{fi})]\rangle \tag{4}$$

is a periodic fluctuating profile around the average $\rho = 1/L^d$ with roughly $\rho/4$ amplitude.

We propose a representation of the GRF that has the structure of (3) and eliminates the above disadvantages:

$$\phi(\mathbf{x}) \approx L^{d/2}\sum_j \zeta_j F(\mathbf{x};\mathbf{s}_j) \tag{5}$$

where the random variables ζ_j are uncorrelated $\langle\zeta_j\zeta_i\rangle = \delta_{i,j}$ and the points $\mathbf{s}_j$ are uniformly random distributed with the average density $\rho = 1/L^d$. This form, Eq. (5), is motivated by its simplicity, and it is able to reproduce the covariance exactly (in contrast with the formula (3)).

In this section, we have shown that an exact, integral, representation of a GRF (1), (2) can be approximated with a discrete version (5) provided that the stochastic character is absorbed as random parameters $\mathbf{s}_j$ of the kernel function $F(\mathbf{x};\mathbf{s}_j)$.

2.2 Gaussian convergence

The discrete form (5) reproduces the exact covariance function even in the limit $L \to \infty$ (a single term in the sum). The limit $L \to 0$ (large $\rho = 1/L^d$) is required in order to achieve the multivariate Gaussian probability distribution function $P(\{\varphi_i\};\{\mathbf{x}_i\}) = \langle\prod_{i=1}^k \delta[\varphi_i - \phi(\mathbf{x}_i)]\rangle$. Our aim is to maximize the convergence rate toward Gaussian character of the series (5) at a fixed density. In other words, we look for representations of $\phi(\mathbf{x})$ that are "Gaussian enough" with a minimal parametric density ρ.

We focus for simplicity further on the one-point PDF $P(\varphi;\mathbf{x}) = \langle\delta[\varphi-\phi(\mathbf{x})]\rangle$. The local rate of convergence for a sum of independent variables is bounded by the Berry–Esseen theorem Korolev and Shevtsova 2010 as $r < C\sigma_3/\sigma_2$, where the constant $C \approx 0.55$ Shevtsova 2014. In our case:

$$\sigma_2^2 = \sum_j \langle|\zeta_j F(\mathbf{x};\mathbf{s}_j)|^2\rangle$$

$$\sigma_3 = max\left(\frac{\langle|\zeta_j F(\mathbf{x};\mathbf{s}_j)|^3\rangle}{\langle|\zeta_j F(\mathbf{x};\mathbf{s}_j)|^2\rangle}\right).$$

In order to reproduce the exact covariance function, σ_2 is constrained to $\sigma_2^2 = 1$. Thus, one can maximize r under the constrain $\sigma_2 = 1$ and obtain through a simple functional calculus that the ζ_j variables must take randomly the ± 1 values, i.e., their PDF is

$$p(\zeta) = \frac{1}{2}(\delta[\zeta+1] + \delta[\zeta-1]). \tag{6}$$

In this section, we have shown that the fastest way for an approximation of the type (5) to acquire Gaussian character is to define the coefficients ζ_j as uniformly distributed stochastic variables with discrete rather than continuous domain.

2.3 Canonically conjugated representations: Fourier & Blob case

The functions $F(\mathbf{x};\mathbf{s})$ (2) are not unique, but are defined up to any unitary transformation $U(\mathbf{x};\mathbf{s})$:

$$F'(\mathbf{x};\mathbf{s}) = \int d\mathbf{s}_1 F(\mathbf{x};\mathbf{s}_1)U(\mathbf{s}_1;\mathbf{s}) \tag{7}$$

$$\delta(\mathbf{s}_1-\mathbf{s}_2) = \int d\mathbf{s}U(\mathbf{s}_1;\mathbf{s})U(\mathbf{s}_2;\mathbf{s}), \tag{8}$$

where $F'(\mathbf{x};\mathbf{s})$ is solution of Eq. (2). We note that $F(\mathbf{x};\mathbf{s})$ can be interpreted either as an operator (the "square root" of the covariance operator $\mathcal{E}(\mathbf{x};\mathbf{y})$) or as a set of parametric functions which reproduces the covariance.

A particularly important unitary transformation is the Fourier transform $U(\mathbf{s}_1;\mathbf{s}) = e^{i\mathbf{s}_1\mathbf{s}}$ which links two sets of **canonically conjugated representations**:

$$F'(\mathbf{x};\mathbf{s}) = \int d\mathbf{s}_1 F(\mathbf{x};\mathbf{s}_1) e^{i\mathbf{s}_1\mathbf{s}} \tag{9}$$

A particularly important representation is suggested by the relation (2) as scaled eigenvectors of the covariance operator $F(\mathbf{x};\mathbf{s}) = \sqrt{\lambda(\mathbf{s})}\psi_{\mathbf{s}}(\mathbf{x})$ where $\psi_{\mathbf{s}}(\mathbf{x})$ is an eigenvector and $\lambda(\mathbf{s})$ its associated eigenvalue $\int d\mathbf{y}\mathcal{E}(\mathbf{x};\mathbf{y})\psi_{\mathbf{s}}(\mathbf{y}) = \lambda(\mathbf{s})\psi_{\mathbf{s}}(\mathbf{x})$. This choice yields the Karhunen–Loeve representation Hua and Liu 1998.

We consider the case of homogeneous GRFs, $\mathcal{E}(\mathbf{x};\mathbf{y}) \equiv \mathcal{E}(\mathbf{x}-\mathbf{y})$. The natural eigenvectors for a translation invariant operator are plane waves $\psi_{\mathbf{k}}(\mathbf{x}) = e^{i\mathbf{k}\mathbf{x}}$ while the corresponding eigenvalues $\lambda(\mathbf{k}) = S(\mathbf{k})$ where $S(\mathbf{k})$ is the spectrum, the Fourier transform of the covariance.

Thus, using the Karhunen–Loeve decomposition and searching for real-valued fields, we obtain a Fourier-like parametric function F_F. Choosing the transformation $U(\mathbf{a};\mathbf{k}) = e^{i\mathbf{a}\mathbf{k}}$, one gets from F_F the "Blob-function" F_B:

$$\zeta F_F(\mathbf{x};\mathbf{k}) \equiv \sqrt{S(\mathbf{k})} sin(\mathbf{k}\mathbf{x} + \frac{\pi}{4}\zeta)$$
$$F_B(\mathbf{x};\mathbf{a}) = \int d\mathbf{k}\sqrt{S(\mathbf{k})} e^{-i\mathbf{k}\mathbf{x}} e^{i\mathbf{k}\mathbf{a}} \equiv F_B(\mathbf{x}-\mathbf{a}).$$

Introducing these functions in the approximative discrete form derived (5), we obtain **the canonically conjugated Fourier and Blob representations**

$$\phi_F(\mathbf{x}) \approx L_k^{d/2} \sum_{j=1}^{N_c} \sqrt{S(\mathbf{k}_j)} sin(\mathbf{k}_j\mathbf{x} + \frac{\pi}{4}\zeta_j) \tag{10}$$

$$\phi_B(\mathbf{x}) \approx L_a^{d/2} \sum_{j=1}^{N_c} \zeta_j F_B(\mathbf{x}-\mathbf{a}_j) \tag{11}$$

which differ from the discrete Fourier decomposition (FFT) or the discrete Moving-Average methods (MA) Ravalec et al. 2000 through the use of stochastic wave numbers $\mathbf{k}_j$, blob positions $\mathbf{a}_j$ and discrete values for the stochastic phases and blob amplitudes $\zeta_j = \pm 1$.

The series (5) becomes finite if the functions $F(\mathbf{x};\mathbf{s})$ have a compact support in the parametric space $\mathbf{s}$. Consequently, the number of terms in the sum N_c is roughly the ratio between the volume of the compact support and the chosen density of parameters ρ.

For the Fourier representation (10), the compact support is the domain in the reciprocal space $\{\mathbf{k}_i\}$ where the spectrum $S(\mathbf{k}_i)$ has non-negligible values. For the Blob representation (11), the compact support is the domain in the real space $\{\mathbf{a}_i\}$ where the blob function $F_B(\mathbf{x}-\mathbf{a}_i)$ has non-negligible values. Thus, these two methods require a similar number of terms N_c in the sum in order to calculate a realization of the field in a point $\mathbf{x}$ with a given accuracy. We note that the usual discrete Fourier decomposition (with fixed grid points) usually needs larger values of N_c, as demonstrated in the next section.

In this section, we have shown that the Fourier (10) and Blob (Moving-Average) (11) are complementary, canonically conjugated, representations. Thus, we expect them to capture different physical features when applied to transport problems such as V-Langevin equations.

2.4 Advantages of the Fourier and Blob representations

The FFT approach is usually considered as one of the fastest construction techniques for GRFs. It allows one to compute the values of the field $\phi(\mathbf{x})$ on a physical, equidistant grid, of dimension N_g using N_g equidistant wavenumbers, with a numerical complexity $\mathcal{O}(N_g \log N_g)$. Using the Fourier/Blob methods (10), (11) with random $\{\mathbf{k}_i\}/\{\mathbf{a}_i\}$ to compute the values on the same grid requires a computational cost which scales as $\mathcal{O}(N_g \times N_c)$ where N_c is the number of parameters considered in the compact support. In general, we expect $\log N_g \ll N_c$. Even in this context, the proposed methods are particularly tempting because:

1. The randomness of the parameters improves the convergence rates toward Gaussianity, such that N_c is required to be only a few times larger than $\log N_g$ (especially in low dimensional spaces $d = 1, 2$).
2. The randomness of the parameters improves the way the parametric space is spanned, allowing for smooth convergent covariance for any number of terms in the series. FFT needs dense grids to achieve that.
3. The resulting fields are not spatially periodic.
4. The GRFs have a preserved structure of the equipotential or contour lines (no interpolation needed for the field values in-between grid points).

The disadvantages are that the random parameters must be generated at every realization. The Blob method requires a supplementary implementation of a nearest neighbor algorithm. The Blob method might not have always analytical Blob functions which may obstruct partially its applicability as it would require numerical interpolation techniques.

3 Accuracy study and DNS tests

The Fourier (10) and Blob (11) representations are tested in the case of a 2D homogeneous GRF with the covariance

$$\mathcal{E}(x,y) \equiv \langle \phi(\mathbf{x}')\phi(\mathbf{x}'+\mathbf{x}) \rangle = \exp\left(-\frac{x^2}{2\lambda_x^2} - \frac{y^2}{2\lambda_y^2}\right), \tag{12}$$

which yields the associated Blob functions

$$F_B(x, y) = \sqrt{\frac{2}{\pi \lambda_x \lambda_y}} \exp\left(-\frac{x^2}{\lambda_x^2} - \frac{y^2}{\lambda_y^2}\right). \tag{13}$$

The correlation lengths are chosen $\lambda_x = 0.3$, $\lambda_y = 0.4$. The Fourier's compact support is a rectangle in which $|\mathbf{k}_i|\lambda_i \leq 5$ which ensures that 99.91% of the spectrum is reproduced. The Blob's compact support is a rectangle in which $|\mathbf{a}_i|/\lambda_i \leq 4$ which ensure that 99.99% of the covariance is reproduced.

More precisely, we investigate numerically the effects of the additional stochastic elements introduced in the representations (10) and (11) and the ability of the simple discrete distribution (6) to improve the convergence rate. For that, we shall use, further, six methods of computing the GRF, which are described in Table 1. The notation for each type of representation consists of three characters: the first letter for the method (Fourier or Blob), the second for how the parameters are distributed (Fixed or Random) and the third for the distribution of the random phases ζ (Continuous or Discrete distributions).

3.1 Reproducing the covariance

We construct an ensemble of $M = 10^3$ realizations of the GRF $\phi(\mathbf{x})$ with the covariance (12) on a rectangular domain $[-\pi, \pi] \times [-\pi, \pi]$ using all six methods. A small number of parametric points $N_c = 12^2$ in the compact support was chosen for each method. The fluctuations of the resulting covariance around the exact profile $\delta\mathcal{E}(\mathbf{x}) = \langle\phi(\mathbf{0})\phi(\mathbf{x})\rangle - \mathcal{E}(\mathbf{x})$ can be seen in Fig. 1. All methods offer similar amplitudes except the FFC method, which, due to its fixed equidistant grid in the $\mathbf{k}$ space has an unphysical periodicity.

The rate of convergence for the error of the covariance function $|\delta\mathcal{E}| = \int |\mathcal{E}(\mathbf{x}) - \mathcal{E}_{approx}(\mathbf{x})| d\mathbf{x}$ can be seen in Fig. 2 ($N_c = 12^2$) as function of M, the ensemble dimension. One can see that $|\delta\mathcal{E}|$ decays with the increase of M at approximately the same rate for five of the above methods and that the FFC (standard FFT) has a much weaker convergence at small values of N_c. These five methods are able to reproduce the covariance even at small values of the number of elements in the sums in Eqs. (10), (11). On the contrary, the FFC method (standard FFT) offers a poor representation of the covariance function on grids with low densities of points, in comparison with the other proposed methods. Increasing N_c, the decay rate of the error increases for the FFC method, but values similar to the other representation are attained at very large N_c (of the order $\sim 100^2$). Essentially, the fail is due to the weak stochastic character of FFC (fixed grid for the wave numbers). We note that the corresponding fixed grid Blob method (the BFC) gives much better results in spite of the same weak stochastic character.

Thus, reasonable values of the error of the convolution are obtained with the FFC method at much larger values of M and/or N_c. The computational time that scales as $M \times N_c$ is much longer for the FFC than for the other five methods (by at least one order of magnitude).

3.2 Reproducing the Gaussian character

We have generated large ensembles ($M = 10^7$) of GRFs with all methods using even fewer points $N_c = 5^2$. In order to test the Gaussianity of the resulting fields, we have focused mainly on the one-point PDF of the field $\phi(\mathbf{0})$. We note that much larger values of M are necessary in order to reduce the statistical fluctuations in the computed PDFs. The results are presented in Fig. 3. One can see that the FFC has low quality for the potential distribution, as for the covariance function (Fig. 1). The corresponding Blob representation (with fixed grid, BFC) is even worse for $P(\phi)$ (see Fig. 3). It is obvious that the use of random grids instead of fixed ones is a much better choice also in the matter of Gaussianity. Moreover, as it has been stated in Sect. 2.2, using discrete distributions $\zeta_j = \pm 1$, instead of distributions with continuous support, offers significant improvements in the profile $P(\phi)$: FRD and BRD are better than FRC and BRC.

Table 2 quantifies these results computing the first even moments for the PDF of $\phi(\mathbf{0})$. The global error defined as $|\delta P| = \int |P_{gauss}(\phi) - P_{method}(\phi)| d\phi$ and the 4-point correlation function $\mathcal{E}_{(4)} = \langle\phi(\mathbf{x}_1)\phi(\mathbf{x}_2)\phi(\mathbf{x}_3)\phi(\mathbf{x}_4)\rangle$ with $\mathbf{x}_1 = (0, 0)$, $\mathbf{x}_2 = (\lambda_x, \lambda_y)$, $\mathbf{x}_3 = (\lambda_x/2, -\lambda_y/3)$, $\mathbf{x}_4 = (-\lambda_x/3, \lambda_y/2)$ are also shown. One can see that fixed grids lead to sub-Gaussian distributions while random grids to over-Gaussian ones (longer tails).

Thus, we have shown that the best choices for the representation of homogeneous GRFs are based on random grids with $\zeta = \pm 1$, i.e., on FRD (10) or BRD (11) methods. Further, by Blob representation we shall refer to BRD while by Fourier to FRD methods in the remaining part of this paper. Note that the Fourier is slightly better than the Blob method.

3.3 DNS of stochastic transport

We have proven until now that the Fourier (10) and Blob (11) representations offer the best convergence rates from the perspective of their Eulerian properties. Now, we perform additional tests regarding their Lagrangian abilities in the context of a DNS of a V-Langevin equation. The following model has been chosen:

$$\frac{d\mathbf{x}(t)}{dt} = \mathbf{v}(\mathbf{x}(t)) = \hat{e}_z \times \nabla\phi(\mathbf{x}(t)) + V_d \hat{e}_y, \tag{14}$$

Table 1 The numerical representations tested in this Section

	FFC	FRC	FRD	BFC	BRC	BRD
Method	Fourier	Fourier	Fourier	Blob	Blob	Blob
Parameters	Fixed	Random	Random	Fixed	Random	Random
ζ	$[0, 8)$	$[0, 8)$	± 1	Gaussian	Gaussian	± 1

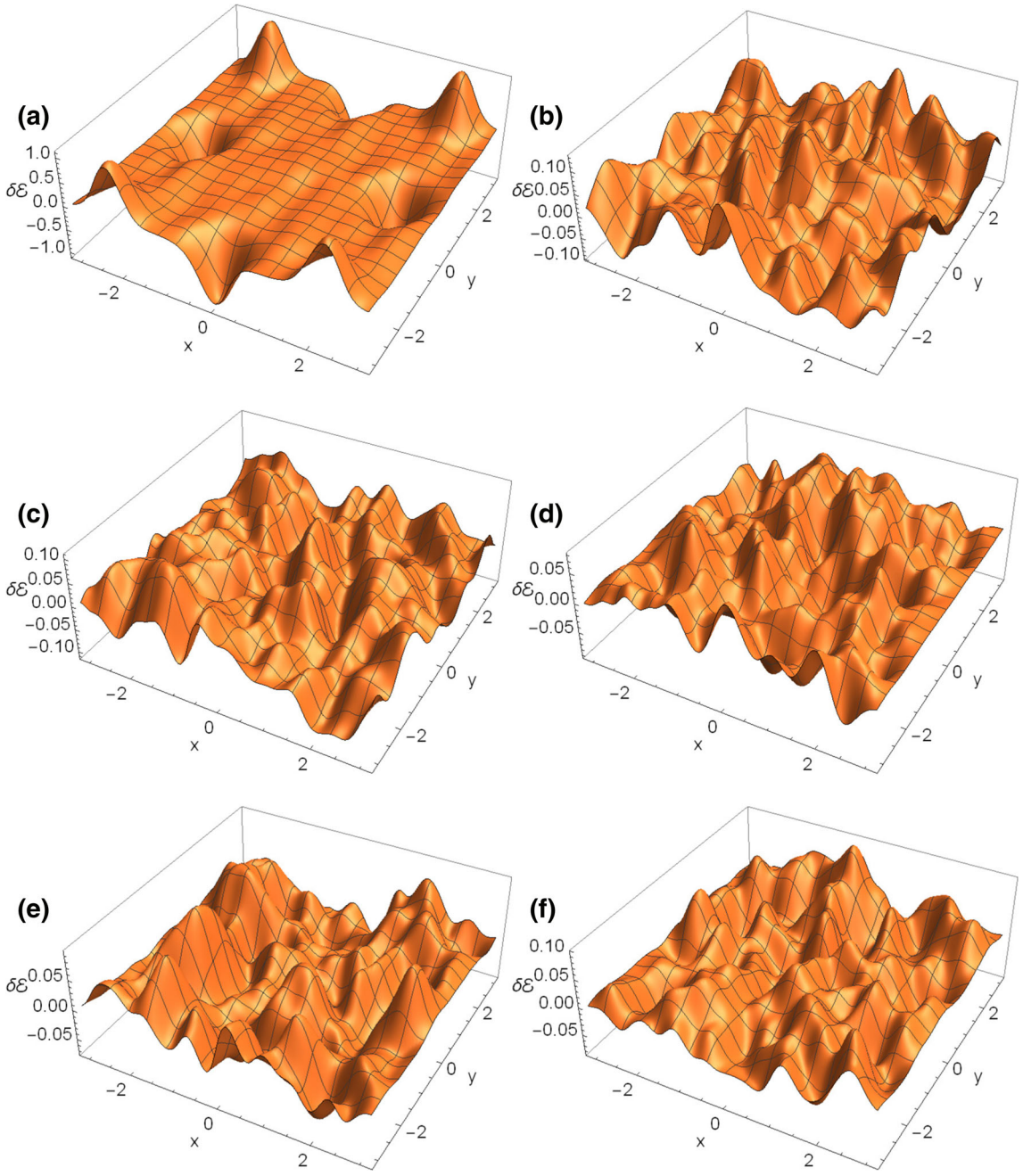

Fig. 1 The error $\delta\mathcal{E}(\mathbf{x})$ of the covariances averaged over ensembles of $M = 1000$ realizations with the FFC (**a**), FRD (**b**), FRC (**c**), BFC (**d**), BRD (**e**), BRC (**f**) methods

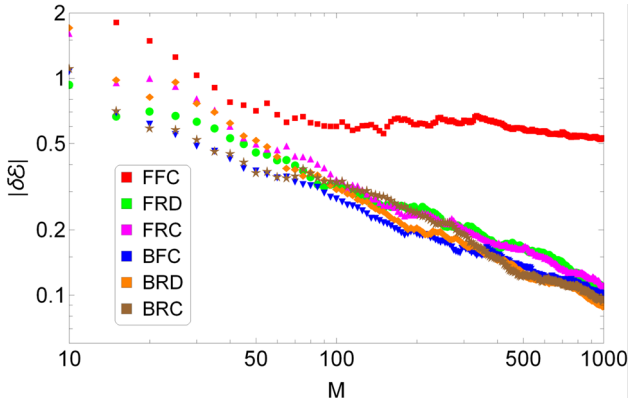

Fig. 2 Evolution of covariance error with the dimension of the ensemble for the FFC (red square), FRD (green circle), FRC (magenta up-triangle), BFC (blue down-triangle), BRD (orange diamond), BRC (brown star) methods. (Color figure online)

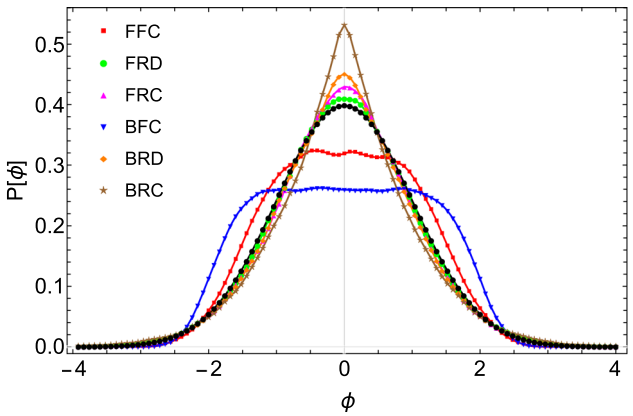

Fig. 3 PDFs of $\phi(\mathbf{0})$ obtained with the FFC (red square), FRD (green circle), FRC (magenta up-triangle), BFC (blue down triangle), BRD (orange diamond), BRC (brown star) methods using $N_c = 5^2$ and a statistical ensemble of $M = 10^7$ realizations. (Color figure online)

where $\phi(\mathbf{x})$ is a GRF and $V_d\hat{e}_y$ is an average velocity. This stochastic equation describes the dynamics of test particles under electrostatic turbulence in magnetically confined plasmas Hauff and Jenko 2006; Vlad et al. 1998; Vlad and Spineanu 2019, the random walk of the magnetic field lines in astrophysics Lazarian and Yuen 2018; Vlad 2018; Snodin et al. 2013 or for tracer transport in incompressible turbulent fluids Haworth and Pope 1986; Kraichnan 1976. The stochastic potential is considered frozen, i.e., the covariance is time independent. The covariance function is (12) with $\lambda_x = 1, \lambda_y = 2$.

We have chosen this transport model because the ensemble of solutions exhibits two invariants: a "local" one characteristic to each trajectory and a global one, characteristic to the entire ensemble. Both are a consequence of the null divergence $\nabla \cdot \mathbf{v}(\mathbf{x}) = 0$ property and of the homogeneity of the stochastic field.

The equation of motion (14) is of Hamiltonian type, with $\phi_t(\mathbf{x}) = \phi(\mathbf{x}) + V_d x$ the Hamiltonian function. The latter is invariant in each realization of the potential $\phi(\mathbf{x})$, since the trajectories obtained from Eq. (14) evolve on the contour lines of $\phi_t(\mathbf{x})$. The structure of the total potential strongly depends on the average velocity V_d. At $V_d = 0$, all the contour lines of the potential (except one) are closed and their sizes have unlimited values (in an infinite plane). All trajectories are trapped on the contour lines; they are periodic functions of time with unlimited periods. In the presence of V_d, the configuration of the contour lines consists of open lines that wind between islands of close lines. As V_d increases the size of the islands decreases, and, at V_d larger than the amplitude of the stochastic velocity, they disappear. The trapping affects only a part of the trajectories, while the others are free (along V_d).

The second invariant is statistical and involves the Lagrangian velocity $\mathbf{v}(\mathbf{x}(t))$. According to Lumley's Theorem Monin 1971, the statistics of the Lagrangian velocity is identical with the statistics of the Eulerian velocity, at any time

$$P^L[\mathbf{v}(\mathbf{x}(t))] = P^E[\mathbf{v}(\mathbf{x})],$$

where $P^L = \langle\delta[\mathbf{v} - \mathbf{v}(\mathbf{x}(t))]\rangle$ is the Lagrangian probability and $P^E = \langle\delta[\mathbf{v} - \mathbf{v}(\mathbf{x})]\rangle$ is the Eulerian probability. The latter is a space-independent Gaussian function

$$P^E(\mathbf{v}) = \exp\left(-\frac{v_x^2}{2V_{xx}} - \frac{(v_y - V_d)^2}{2V_{yy}}\right),$$

where $V_{ii} = \langle v_i(\mathbf{0})v_i(\mathbf{0})\rangle = -\partial_{jj}\mathcal{E}(\mathbf{x})|_{\mathbf{x}\to\mathbf{0}} = 1/\lambda_j^2$.

The existence of the constraints related to these invariants makes the transport process very complicated, but it also provides strong benchmarks for the numerical simulations.

Regarding the numerical implementation, a second-order Runge–Kutta numerical integration scheme has been used for a time interval of $[0, t_{max}] = [0, 40]$ with a fixed time step $dt = 0.04$. An ensemble of $M = 3\times10^4$ trajectories has been resolved. We have implemented the Fourier (FRD) and Blob (BRD) representations with $N_c = 6^2, 12^2$. Two cases have been considered: $V_d = 0$ and $V_d = 0.4$. A Fourier simulation with N_c waves is denoted by FN_c while a Blob one by BN_c where $N_c = 36$ or 144.

We underline that M, the dimension of the ensemble and (especially) N_c, the number of random parameters in the series (10), (11), are small compared to the usual values Manfredi and Dendy 1996 in DNS. Thus, the DNS can be performed on personal computers, where the typical running times are rather small, of the order of $t_{CPU} \sim 10^2 s$.

First, we have checked that the numerical integration and the use of the generators (10), (11) of the GRF do not affect the Hamiltonian character of the trajectories. We plot in Fig.

Table 2 Numerical values of the first odd moments of the PDF $P(\varphi;\mathbf{0})$ for all six methods considered using $N_c = 5^2$

	FFC	FRC	FRD	BFC	BRC	BRD	exact
$<\phi^2>$	1.046	1.002	0.999	1.264	1.001	1.001	1
$<\phi^4>$	2.504	3.424	3.223	3.257	3.976	3.543	3
$<\phi^6>$	8.447	21.32	18.38	11.04	30.83	23.37	15
$<\phi^8>$	35.13	199.82	145.48	44.19	372.89	235.67	105
$\lvert\delta P\rvert$	0.167	0.061	0.026	0.309	0.136	0.066	0
$\mathcal{E}_{(4)}$	0.744	1.041	0.948	0.694	0.906	0.850	0.789

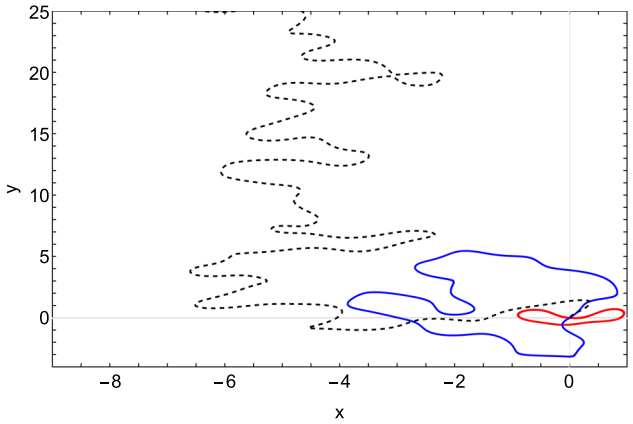

Fig. 4 In red and blue (full line), two closed trajectory simulated for $\approx$ 10 times their periods. In black (dashed line) a free trajectory. All trajectories are obtained for different realizations of the same ensemble in the presence of an effective $V_d = 0.4$

4 three typical trajectories, which illustrate the existence of free and trapped (with different sizes) trajectories obtained from Eq. (14). All are well tied to the contour lines of the potential (even the small one that performs $\approx$ 10 periods). Apart from small oscillations $\delta\phi(t)/\bar{\phi} \sim 10^{-4}$, the potential is perfectly conserved along the represented trajectories. Thus, the combined errors from the approximation of the field and from the numerical integration remain small.

Second, we test the global invariants by computing the PDF of Lagrangian velocities $P^L[\mathbf{v}(\mathbf{x}(t))]$ as well as its first moments $\langle v_i^j(t)\rangle$, $j = 1, 4$. Figure 5 shows the components of this distribution of the Lagrangian velocity at the moment $t = 20$, compared with the exact, Gaussian profiles. The results are close to the theoretical distributions, even for the cases $N_c = 36$. The statistical fluctuations can be analyzed more clearly in Fig. 6 where the moments $\langle v_i^j(t)\rangle$ are shown. On average, the Lagrangian invariance is well reproduced by both methods, the fluctuations being a consequence of a finite ensemble ($M = 3\times10^4$). The deviations of the average values (for example $\langle v_y^4\rangle \approx 3.3$ instead of the exact value 3 for $B36$ method) are a consequence of a finite N_c. As seen in Fig. 6, the increase of N_c approaches the averages to the theoretical values and reduces the statistical fluctuations. The results are satisfactory even at the small values taken here.

The stochastic velocity field prescribed by the V-Langevin Eq. (14) is Gaussian, time-invariant and has null divergence. Yet, the resulting distribution of $P(\mathbf{x}(t)) = \langle\delta[\mathbf{x} - \mathbf{x}(t)]\rangle$ is not a Gaussian function. Instead, at finite times, it is a peaked function which exhibits long tails Vlad and Spineanu 2017 as it can be seen Fig. 7 for $P[x(t)]$. The physical reason is that the trajectory trapping or eddying, produced by the invariance of the Lagrangian potential, ties particle paths on its contour lines. In the presence of an average velocity V_d, part of the contour lines open-up leading to free particles which move along the $\hat{e}_y$) direction, while the rest remain closed being only "elongated." These aspects can be seen in Fig. 7 on the $P[y(t)]$ profile which exhibits two local maxima: one at $y = 0$ for the trapped particles and one slightly above $y = V_d t$ for the free particles.

There are no clear theoretical results on $P(\mathbf{x}(t))$ that could be used as benchmark of the present DNS. Instead, we compare the results of the four runs discussed here. The probability of the displacements $x(t)$ and $y(t)$ is shown in Fig 7. It can be observed that $F144$ and $B144$ provide almost identical profiles. The low-resolution simulations $B36$ and $F36$ deviate in a complementary manner from the $F144/B144$ results. The distributions obtained with $B36$ have larger values of the peaks around $y = 0$ as well as a slightly more pronounced short-range character, pointing towards an overestimation of the trapping. The converse is true for $F36$ simulation.

The time-dependent diffusion coefficients $2D_{ii}(t) = d\left\langle x_i^2(t)\right\rangle/dt$ are presented in Fig. 8 for $V_d = 0$ (upper panels) and $V_d = 0.4$ (lower panels). The decay of D_{ii} at large time is the consequence of trajectory trapping. At $V_d = 0$, the transport is subdiffusive with mean square average displacements that have time increase slower than linear. The average velocity V_d strongly modifies the transport. It is superdiffusive along V_d and subdiffusive along x axis, but with decay in a finite time. This is the effect of the change of the configuration of the contour lines of the total potential produced by V_d.

One can see that all simulations yield practically the same result at $t < 1$ and that significant differences appear at $t > 1$, especially between the calculations at $N_c = 36$ and those at $N_c = 144$. Figure 8 also shows that the $F36$ method underestimates the trapping of particles (it yields a slower

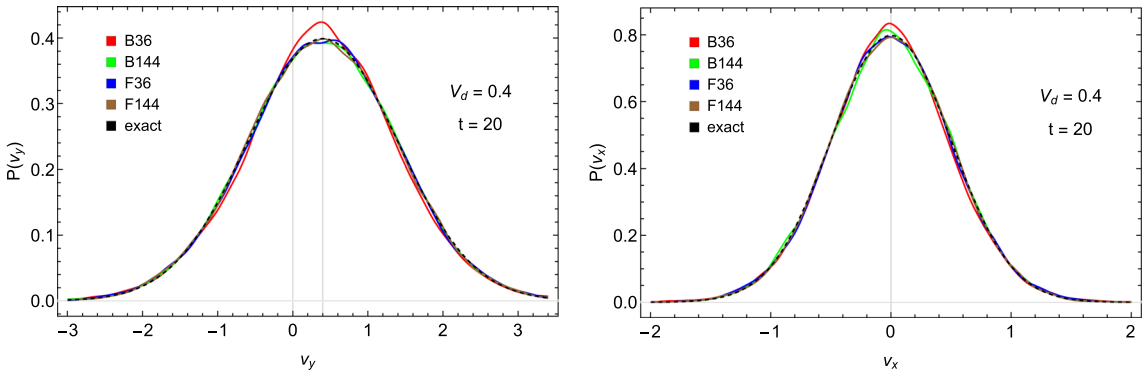

Fig. 5 Large time $t = 20$ distribution of velocities. The exact, Gaussian shapes are in dashed lines

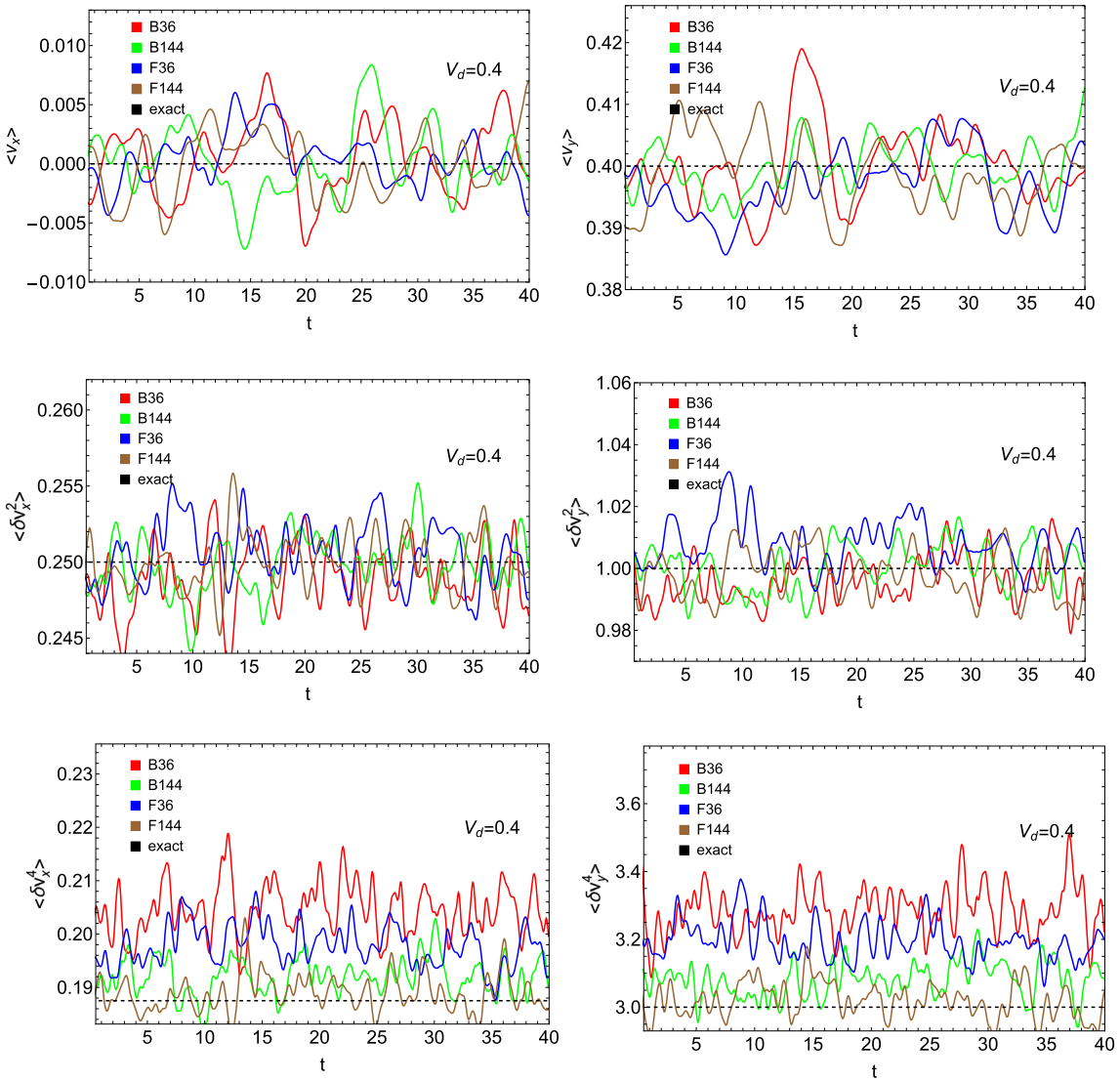

Fig. 6 Time dependence of average Lagrangian velocity moments

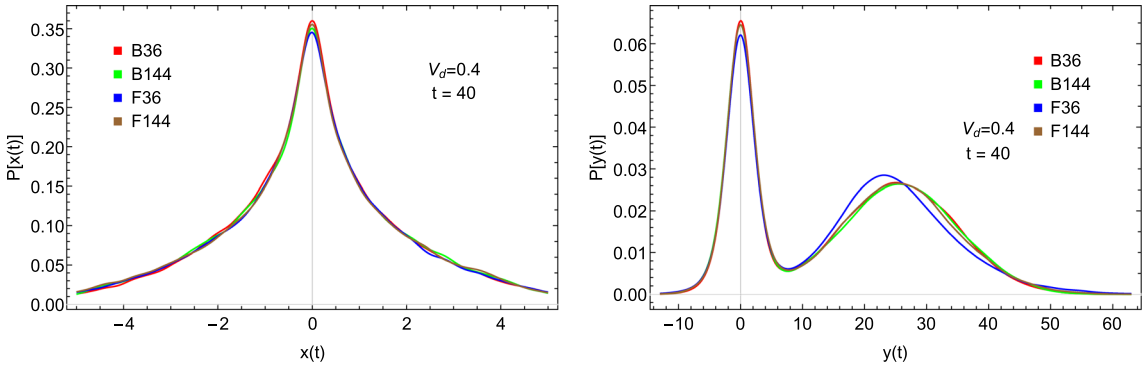

Fig. 7 Projected trajectory distributions $P(x(t))$, $P(y(t))$

decay of D_{ii} at large times $t > 2-3$). The converse is true for the $B36$ method which overestimates the trapping by smaller values of D_{ii} at large times. All methods give a dependence of the diffusion coefficients as $\mathcal{D} \propto t^{\gamma}$. For $F36$ $\gamma \approx -0.15$ while for $B36$ $\gamma \approx -0.4$. At larger values of N_c, $F144$ and $B144$, we can observe how the results and the slope γ converge towards a common profile with $\gamma \approx -0.3$, in accordance with well-known results Isichenko 1992.

3.4 The hybrid representations

The results from Fig. 8 with no bias $V_d = 0$ suggest that there are some intrinsic pathologies within the Fourier and Blob representations. The first seems to produce very long (quasi-free) trajectories, while the latter very small, closed and less complex trajectories. The explanation is related to the specific form of the parametric functions of each representation. Using waves (Fourier) with a small number of terms is more likely to produce long equipotential lines (which are, in fact, trajectories). A single plane wave is unable to produce a closed field line. In contrast, even a single Blob function will generate an inherently closed trajectory. A small number of Blob functions is unlikely to produce long equipotential lines.

Also, Table 2 suggests that the Blob method reproduces better than the Fourier method the higher-order correlations ($\mathcal{E}_{(4)}$). The overestimation of these correlations corresponds to smoother fields, which means less complex fields. But a less complex field has less complex equifieldlines and, consequently, less complex Lagrangian solutions. The overestimation of the correlation in the Fourier representation is natural: the waves are omnipresent, thus, any two points are "correlated" through the wave. Only the statistical averaging of the phases can decouple them.

These shortcomings do not affect the Lagrangian distribution of velocities or the average velocity of the ensemble, as seen in Figs. 5, 6. Their effect is visible in the diffusion coefficients, which show a much stronger dependence on N_c.

These structural properties of the Blob and Fourier methods can be exploited to yield improved results for the diffusion coefficients without increasing N_c. We propose a hybrid representation of the GRF that combines the Fourier and Blob methods:

$$\phi_{FB}(\mathbf{x}) = \eta_1 \phi_F(\mathbf{x}) + \eta_2 \phi_B(\mathbf{x}). \tag{15}$$

with $\eta_1^2 + \eta_2^2 = 1$. We show that the systematic errors of the two methods compensate in this Fourier–Blob (FB) representation. The results obtained for $\eta_1 = \eta_2 = 1/\sqrt{2}$ using the Fourier–Blob approach (15) with $N_c = 36$ are shown in Fig. 9 for the diffusion coefficient $D_{yy}(t)$. The resulting profile is very close to the profiles obtained with $F144$ and $B144$ simulations at any time.

We note, without any graphic representation, that the hybrid method corrects also the displacement distributions $P[x(t)]$, $P[y(t)]$. This behavior is to be expected since the diffusion coefficients are directly connected to the distributions. Technically, it can be understood that the hybrid representation averages between overestimation and underestimation of trapping brought by the Blob, respectively, Fourier representation.

We summarize the hierarchical speed-ups brought by the representations discussed in the present paper. Working with a small $N_c \sim 10^d$, and fixed grids (FFC) is the representation which performs the worst with regard to computational time (Fig. 1). Blob method with fixed grid (BFC) works also poorly from the perspective of Gaussianity (Fig. 3). Using random grid elements (FRC or BRC) leads to an increase in the convergence rates (Fig. 3, Table 2), thus to an order of magnitude increase in the speed-up of these methods. Using, as proven, discrete values of the phases ζ (FRD, BRD) adds a small refinement in the Gaussian character of the fields (Fig. 3, Table 2), consequently a small increase in speed-up. The Lagrangian perspective shows that we can use for DNSs of V-Langevin equations the hybrid approach which averages between the flaws of Fourier and Blob methods to cut the numerical effort in half. Thus, the hybrid method is roughly twice as fast than (FRC,FRD,BRC,BRD) methods which are

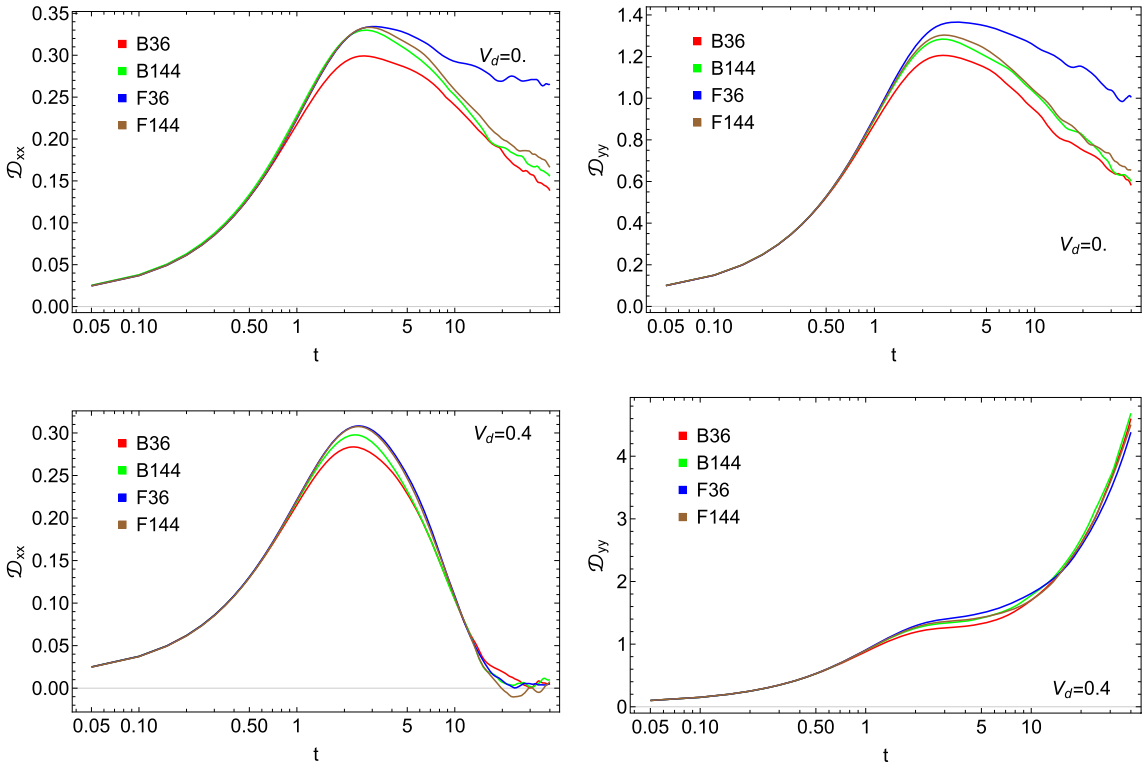

Fig. 8 Diffusion coefficients $\mathcal{D}_{ii}(t)$ obtained with the methods B36 (red), F36 (blue), B144 (green), F144 (brown). (Color figure online)

roughly one order of magnitude faster than the (FFC,BFC) standard representations.

3.5 Long range and time-dependent GRFs

Although the Gaussian covariance (12) is relevant for a large class of physical systems, we must recognize that it has a particularity: it is a short-ranged function. Consequently, the associated random fields do not exhibit simultaneously multiple scale structures. Thus, one might argue that this is the reason why the Fourier–Blob hybrid method behaves so well.

In order to investigate further the applicability of our proposal, we choose a different case of covariance which is both long-range and time dependent:

$$\mathcal{E}(\mathbf{x},t) \equiv \langle \phi(\mathbf{x}',t')\phi(\mathbf{x}'+\mathbf{x},t'+t)\rangle = \left(1+|\mathbf{x}|^2\right)^{-3/2} \exp\left(-\frac{t^2}{4\tau_c^2}\right). \tag{16}$$

The potential is a three-dimensional stochastic field (two space dimensions and time), so that this case also exemplifies the behavior of the GRFs generators at higher dimension (the transport in a more complex system with 4D GRF generators was recently studied using the results presented here Vlad et al. 2020). For this case, we can compute analytically both the associated spectrum and the Blob function:

$$S(\mathbf{k},\omega) = \frac{\tau_c}{2\pi^{3/2}} e^{-|\mathbf{k}|-\omega^2\tau_c^2} \tag{17}$$

$$F_B(\mathbf{x},t) = \sqrt{\frac{8\pi^{3/2}}{\tau_c}} \left(1+4|\mathbf{x}|^2\right)^{-3/2} \exp\left(-\frac{t^2}{2\tau_c^2}\right) \tag{18}$$

The V-Langevin Eq. (14) require the computation of field derivatives $\partial_i\phi(\mathbf{x},t)$; consequently, we need a good representation not only of the field itself, but of the derivatives too. In terms of Fourier-like representations, this implies that the weighted spectrum $S(\mathbf{k},\omega)|\mathbf{k}|^2$ (the spectrum of derivatives) must be well captured. But, to do that, in the case of an exponential space spectrum $\exp(-|\mathbf{k}|)$ we need to enlarge the compact support in the reciprocal space. In practice, we use $|\mathbf{k}_i| \leq 10$ to recover 99.9%, respectively, 98.9% from the amplitude of field fluctuations $\langle\phi(\mathbf{0},0)^2\rangle$, respectively, derivative fluctuations $\langle[\partial_x\phi(\mathbf{0},0)]^2\rangle$. It is interesting that, in order to recover the same quantities within Blob representation, one does not need an enlarged compact support. The latter is rather defined by the regions in space for which the values of the function itself can be neglected. In practice, we choose $|\mathbf{a}_j| \leq 2.5$ which introduces errors of $\sim 1\%$.

Thus, we expect that Fourier-like methods will require a larger number of elements N_c in the long-ranged case than they did in the Gaussian case. We test this idea in Fig. 10 where we have plotted the distribution of one-point values of the fields $P[\phi(0)]$ obtained with all types of representations at $N_c = 5^3$. The typical accuracy behavior found in Fig. 3

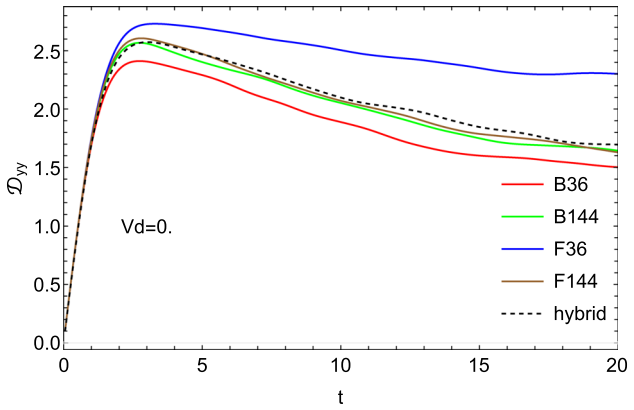

Fig. 9 The diffusion coefficient D_{yy} obtained with the Fourier-Blob representation (15) with $N_c = 36$ (for both Fourier and Blob terms) compared to the results presented in Fig. 8

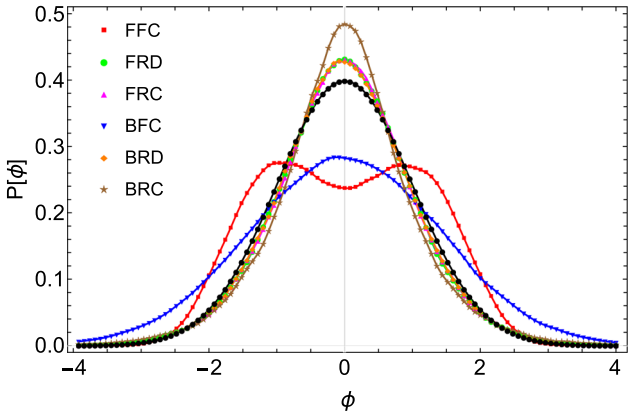

Fig. 10 PDFs of $\phi(\mathbf{0})$ obtained with the FFC (red square), FRD (green circle), FRC (magenta up-triangle), BFC (blue down triangle), BRD (orange diamond), BRC (brown star) methods at $N_c = 5^3$ and a statistical ensemble of $M = 10^7$ realizations. (Color figure online)

is reproduced also in this long-range, time-dependent case. In particular, one can see how the FRD (green circle) and BRD (orange diamond) are the closest profiles to the Gaussian distribution (exact, black circles) in agreement with the theoretical expectations. Moreover, in contrast with Fig. 3, here, the FRD and BRD representations offer similar accuracy levels.

Note that in this 3D case, with long-range space correlation, using $N_c \sim 5^3$ deviates further from Gaussianity than it did in the short-ranged case. This can be seen qualitatively comparing Figs. 3, 4, 5, 6, 7, 8, 9, 10 and Tables 2–3. Therefore, we expect that pertinent descriptions of ensemble statistics should be obtained with at least $N_c \sim 10^3$. Considering that generic ensembles used in DNS should contain $M \sim 10^5$ trajectories and an usual number of times steps required is $N_t \sim 10^3$, one can see how the number of operations involved in a single DNS can be a matter of concern. Consequently, increasing by a factor of two the computational speed becomes important.

We proceed further to test the FRD, BRD and the hybrid method for DNSs of V-Langevin Eq. (14). We use $\tau_c = 1$ and $V_d = 0$. From a physical point of view, the time dependence of the fields $\phi(x(t), t)$ breaks the local Lagrangian conservation of the potential. The trajectories are no longer closed, even in the absence of V_d, being rather a series of jumps between quasi-trapped states. Consequently, we expect that time variation will be equivalent with a decorrelation mechanism which will lead to a finite asymptotic diffusion coefficient. In contrast, the frozen-turbulence case (Sect. 3.3, Fig. 8) leads to time decaying diffusions which, asymptotically, become zero.

We perform two types of simulations: with $N_c = 6^3$ and with $N_c = 14^3$. The hybrid method is implemented using $N_c = 9^3 \approx 14^3/4$ and all DNSs simulate $M = 3 \times 10^4$ trajectories. In accordance with Lumley's theorem Monin and Yaglom 2013; Gleeson 2002, the distribution of velocities remains a global invariant even in the time-dependent case. To test this, we plot in Fig. 11 the average Lagrangian velocity and the Lagrangian velocity dispersion and observe how, aside from statistical fluctuation, these quantities remain invariant in time.

Figure 12 shows the running diffusion coefficients obtained with $F6^3$, $B6^3$, $F14^3$, $B14^3$ and the hybrid method with $N_c = 9^3$. As suggested by the Eulerian results (Fig. 10 and Table 3), the long-range character requires a larger numbers of elements N_c to be well represented. This is obvious in Fig. 12 where $D_{xx}(t)$ obtained with $N_c = 6^3$ does not even reach a saturation point. Thus, we have been forced to use $N_c = 14^3$ which seems to be large enough in order for the results to converge toward an asymptotically constant diffusion. The hybrid method is able to reproduce that profile with roughly half the number of elements required by either Fourier or Blob methods.

All methods require a larger N_c and M for accurate DNSs results in the long-range and time-dependent case of field presented in this section. This can also be seen from the statistical fluctuations which are present in the diffusion profiles. Yet, we conclude that the hybrid method's ability to improve the computing time with a rough factor of two is a strong feature valid for more complicated transport problems with higher dimensions and long-range correlations.

4 Summary and conclusions

The general integral representation of the GRFs (1), (2) contains a parametric function $F(\mathbf{x}; \mathbf{s})$ and an uncorrelated random variable $\zeta(\mathbf{s})$. We have derived from Eqs. (1), (2) a set of discrete representations. They are of Blob and Fourier type, according to the parametric function that is a space structure $F_B\left(\mathbf{x} - \mathbf{a}_j\right)$ in the first case and a wave amplitude structure in the second case $F_F\left(\mathbf{x}; \mathbf{k}_j\right) = \sqrt{S(\mathbf{k}_j)} sin(\mathbf{k}_j \mathbf{x})$. Additional

Table 3 Numerical values of the first odd moments of the PDF $P(\varphi;\mathbf{0})$ for all six methods considered using $N_c = 5^3$

	FFC	FRC	FRD	BFC	BRC	BRD	exact
$<\phi^2>$	1.446	1.001	0.999	1.369	1.001	1.001	1
$<\phi^4>$	4.004	3.542	3.576	18.141	4.732	3.565	3
$<\phi^6>$	15.842	23.96	24.86	111.04	49.83	24.232	15
$<\phi^8>$	78.133	254.82	267.83	1344.19	913.32	262.01	105
$\lvert\delta P\rvert$	0.352	0.073	0.076	0.433	0.185	0.078	0

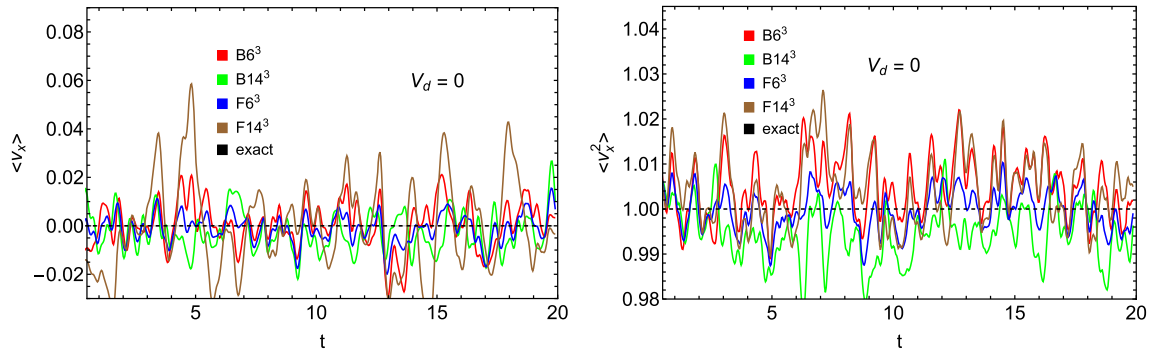

Fig. 11 Time dependence of average Lagrangian velocity moments

stochastic elements were introduced in both types of representations by considering the points $\mathbf{a}_j$ and the wave numbers $\mathbf{k}_j$ as stochastic parameters with uniform distributions. The random variable ζ was taken with discrete ($\zeta = \pm 1$) support.

Six representations of the GRF, defined in Table 1, were analyzed to prove that our proposal Fourier (FRD) and Blob (BRD) provide a better convergence of the Eulerian properties than other standard representations. We have shown that reasonable errors in the covariance and in the PDF of the potential are obtained at much smaller values of N_c and M than in the usual Fourier representation (FFC). This leads to the decrease in the computing times by at least one order of magnitude compared to the usual FFC method.

The convergence of the Lagrangian properties of these two methods was further analyzed in the frame of the DNS of a special type of stochastic transport described by a V-Langevin equation in two-dimensional, time-independent velocity fields with zero divergence. The invariance of the Lagrangian potential in each realization and the statistical invariance of the Lagrangian velocity provide benchmarks for the validation of the numerical results. We have shown that simulations with both Fourier and Blob methods satisfy these constraints with good precision for $N_c \gtrsim 100$ and $M \gtrsim 10^4$. The main difference between these representations appears in their ability to describe the effects of trajectory trapping or eddying on the contour lines of the potential.

The Fourier (FRD) results underestimate, while the Blob (BRD) method overestimates the effects of trapping on the diffusion coefficients. These systematic errors were strongly

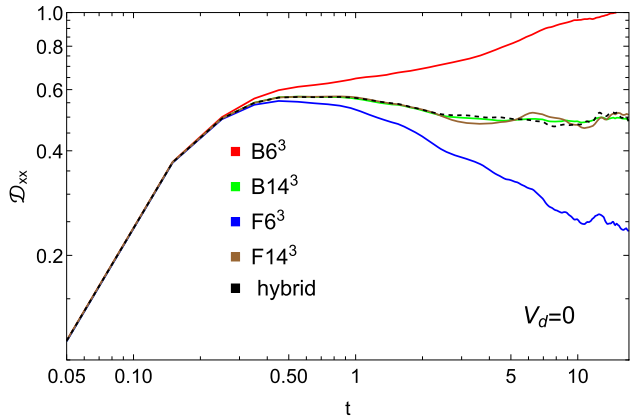

Fig. 12 The diffusion coefficient D_{yy} obtained with the Fourier–Blob representation (15) with $N_c = 9^3$ (for both Fourier and Blob terms) compared to the results obtained with $B6^3$, $F6^3$, $B14^3$, $F14^3$

reduced by a hybrid representation which combines linearly the Fourier and Blob series in a single Fourier–Blob method.

In conclusions, we have strongly improved the representation of the GRFs by introducing additional random elements. We have shown that the hybrid Fourier–Blob method (15) provides a fast tool that can be used in the numerical studies of complex stochastic advection processes. To summarize, the hybrid method is roughly twice as fast than (FRC,FRD,BRC,BRD) methods which are roughly one order of magnitude faster than the (FFC,BFC) standard representations. This opens the possibility of performing such studied on personal computers. For the cases analyzed here, typical

running times are of the order of $10^2 s$ for the 2D case (Sect. 3.4) and $10^3 s$ for the 3D case (Sect. 3.5).

Acknowledgements This work has been carried out within the framework of the EUROfusion Consortium and has received funding from the Euratom research and training programme 2014–2018 and 2019–2020 under grant agreement No 633053 and also from the Romanian Ministry of Research and Innovation. The views and opinions expressed herein do not necessarily reflect those of the European Commission.

References

Abrahamsen, P.: A review of Gaussian random fields and correlation functions. Norsk Regnesentral/Norwegian Computing Center, Oslo (1997)

Balescu, R.: Aspects of Anomalous Transport in Plasmas. CRC Press, Flroida (2005)

Balescu, R.: V-Langevin equations, continuous time random walks and fractional diffusion. Choas Solitons Fractals **34**(1), 62 (2007). https://doi.org/10.1016/j.chaos.2007.01.050

Balescu, R., Wang, H., Misguich, J.H.: Langevin equation versus kinetic equation: subdiffusive behavior of charged particles in a stochastic magnetic field. Phys. Plasmas **1**(12), 3826 (1994). https://doi.org/10.1063/1.870855

Bevilacqua, M., Gaetan, C.: Comparing composite likelihood methods based on pairs for spatial Gaussian random fields. Stat. Comput. **25**(5), 877 (2015). https://doi.org/10.1007/s11222-014-9460-6

Boivin, M., Simonin, O., Squires, K.D.: Direct numerical simulation of turbulence modulation by particles in isotropic turbulence. J. Fluid Mech. **375**, 235–263 (1998). https://doi.org/10.1017/S0022112098002821

Bressloff, P.: Stochastic Processes in Cell Biology. Springer, Cham (2014)

Chan, G., Wood, A.T.A.: Simulation of stationary Gaussian vector fields. Stat. Comput. **9**(4), 265 (1999). https://doi.org/10.1023/A:1008903804954

Cuevas, F., Allard, D., Porcu, E.: Fast and exact simulation of gaussian random fields defined on the sphere cross time. Stat. Comput. **30**(1), 187 (2020)

Diekmann, A., Mitter, P.: Stochastic Modelling of Social Processes. Academic Press, Cambridge (2014)

Ganapathysubramanian, B., Zabaras, N.: A stochastic multiscale framework for modeling flow through random heterogeneous porous media. J. Comput. Phys. **228**(2), 591 (2009)

Ghahramani, Z., Hinton, G.E.: Variational learning for switching state-space models. Neural Comput. **12**(4), 831 (2000). https://doi.org/10.1162/089976600300015619

Gleeson, J.P.: Comment on Diffusion in biased turbulence. Phys. Rev. E **66**, 038301 (2002). https://doi.org/10.1103/PhysRevE.66.038301

Hauff, T., Jenko, F.: Turbulent ExB advection of charged test particles with large gyroradii. Phys. Plasmas (2006). https://doi.org/10.1063/1.2360173

Haworth, D.C., Pope, S.B.: A generalized Langevin model for turbulent flows. Phys. Fluids **29**(2), 387 (1986). https://doi.org/10.1063/1.865723

Higdon, D.: Quantitative Methods for Current Environmental Issues, pp. 37–56. Springer, London (2002)

Hoef, J.M.V., Cressie, N., Barry, R.P.: Flexible spatial models for kriging and cokriging using moving averages and the fast fourier transform (FFT). J. Comput. Graph. Stat. **13**(2), 265 (2004). https://doi.org/10.1198/1061860043498

Hofmann, T., Schölkopf, B., Smola, A.J.: Kernel methods in machine learning. Ann. Stat. **36**(3), 1171 (2008)

Hua, Y., Liu, W.: Generalized Karhunen-Loeve transform. IEEE Signal Process. Lett. **5**(6), 141 (1998). https://doi.org/10.1109/97.681430

Isichenko, M.B.: Percolation, statistical topography, and transport in random media. Rev. Mod. Phys. **64**, 961 (1992). https://doi.org/10.1103/RevModPhys.64.961

Kampen, N.G.: Tochastic Processes in Physics and Chemistry. Elsevier, Amsterdam, Boston, London (2007)

Korolev, V.Y., Shevtsova, I.G.: On the upper bound for the absolute constant in the Berry-Esseen inequality. Theory Probab. Appl. **54**(4), 638 (2010). https://doi.org/10.1137/S0040585X97984449

Kraichnan, R.H.: Diffusion of passive-scalar and magnetic fields by helical turbulence. J. Fluid Mech. **77**(4), 753–768 (1976). https://doi.org/10.1017/S0022112076002875

Krishnamachari, S., Chellappa, R.: Multiresolution Gauss-Markov random field models for texture segmentation. IEEE Trans. Image Process. **6**(2), 251 (1997)

Lazarian, A., Yuen, K.H.: Tracing magnetic fields with spectroscopic channel maps. Astrophys. J. **853**(1), 96 (2018). https://doi.org/10.3847/1538-4357/aaa241

Liu, Y., Li, J., Sun, S., Yu, B.: Advances in Gaussian random field generation: a review. Comput. Geosci. **23**(5), 1011 (2019). https://doi.org/10.1007/s10596-019-09867-y

Manfredi, G., Dendy, R.O.: Test-particle transport in strong electrostatic drift turbulence with finite larmor radius effects. Phys. Rev. Lett. **76**, 4360 (1996). https://doi.org/10.1103/PhysRevLett.76.4360

Monin, A.S.: Statistical Fluid Mechanics: Mechanics of Tribulence. MIT Press, Cambridge, Mass (1971)

Monin, A.S., Yaglom, A.M.: Statistical fluid mechanics, volume: II mechanics of turbulence, pp. 55–99. Courier Corporation, North Chelmsford (2013)

Naulin, V., Nielsen, A.H., Rasmussen, J.J.: Dispersion of ideal particles in a two-dimensional model of electrostatic turbulence. Phys. Plasmas **6**(12), 4575 (1999). https://doi.org/10.1063/1.873745

Paul, W.: Stochastic Processes : From Physics to Finance. Springer, Berlin New York (2013)

Pozorski, J., Minier, J.P.: On the Lagrangian turbulent dispersion models based on the Langevin equation. Int. J. Multiph. Flow **24**(6), 913 (1998). https://doi.org/10.1016/S0301-9322(98)00016-0

Radivojević, T., Akhmatskaya, E.: Modified Hamiltonian Monte Carlo for Bayesian inference. Stat. Comput. **30**(2), 377 (2020)

Ravalec, M.L., Noetinger, B., Hu, L.Y.: The FFT moving average (FFT-MA) generator: an efficient numerical method for generating and conditioning Gaussian simulations. Math. Geol. **32**(6), 701 (2000). https://doi.org/10.1023/A:1007542406333

Reuss, J.D., Misguich, J.H.: Low-frequency percolation scaling for particle diffusion in electrostatic turbulence. Phys. Rev. E **54**, 1857 (1996). https://doi.org/10.1103/PhysRevE.54.1857

Shevtsova, I.G.: On the absolute constants in the Berry-Esseen-type inequalities. Dokl. Math. **89**(3), 378 (2014). https://doi.org/10.1134/S1064562414030338

Snodin, A.P., Ruffolo, D., Oughton, S., Servidio, S., Matthaeus, W.H.: Magnetic field line random walk in models and simulations of reduced magnetohydrodynamic turbulence. Astrophys. J. **779**(1), 56 (2013). https://doi.org/10.1088/0004-637x/779/1/56

Solin, A., Särkkä, S.: Hilbert space methods for reduced-rank Gaussian process regression. Stat. Comput. **30**(2), 419 (2020)

Tautz, R.: On simplified numerical turbulence models in test-particle simulations. J. Comput. Phys. **231**(14), 4537 (2012). https://doi.org/10.1016/j.jcp.2012.02.021

Tautz, R.C., Dosch, A.: On numerical turbulence generation for test-particle simulations. Phys. Plasmas **20**(2), 022302 (2013). https://doi.org/10.1063/1.4789861

Vlad, M., Palade, D., Spineanu, F.:Effects of the parallel acceleration on heavy impurity transport in turbulent tokamak plasmas, Plasma Phys. Control. Fusion **63** 035007 (2021)

Vlad, M.: Effects of the mean field gradients on magnetic field line random walk. Astrophys. J. **867**(2), 104 (2018)

Vlad, M., Spineanu, F.: Random and quasi-coherent aspects in particle motion and their effects on transport and turbulence evolution. New J. Phys. **19**(2), 025014 (2017). https://doi.org/10.1088/1367-2630/aa602d

Vlad, M., Spineanu, F.: Hidden drifts in turbulence. EPL (Europhys. Lett.) **124**(6), 60002 (2019). https://doi.org/10.1209/0295-5075/124/60002

Vlad, M., Spineanu, F., Misguich, J.H., Balescu, R.: Diffusion with intrinsic trapping in two-dimensional incompressible stochastic velocity fields. Phys. Rev. E **58**, 7359 (1998). https://doi.org/10.1103/PhysRevE.58.7359

Vlad, M., Spineanu, F., Croitoru, A.: Nonlinear effects in particle transport in stochastic magnetic fields. ApJ **815** 11(2015). https://doi.org/10.1088/0004-637X/815/1/11

Won, A.Y., Pires, J.A., Haroun, M.A.: Stochastic seismic performance evaluation of tuned liquid column dampers. Earthq. Eng. Struct. Dyn. **25**(11), 1259 (1996)

Wong, E.: Homogeneous Gauss-Markov random fields. Ann. Math. Stat. **40**(5), 1625 (1969)

Yang, D., Shen, L.: Direct numerical simulation of scalar transport in turbulent flows over progressive surface waves. J. Fluid Mech. **819**, 58 (2017)

Zimbardo, G., Veltri, P., Basile, G., Principato, S.: Anomalous diffusion and Lévy random walk of magnetic field lines in three dimensional turbulence. Phys. Plasmas **2**(7), 2653 (1995). https://doi.org/10.1063/1.871453